Bioorganic & Medicinal Chemistry 23 (2015) 4462–4471

Contents lists available at ScienceDirect

Bioorganic & Medicinal Chemistry

journal homepage: www.elsevier.com/locate/bmc

Crystal structures of the apo form and a complex of human LMW-PTP with a phosphonic acid provide new evidence of a secondary site potentially related to the anchorage of natural substrates ☆

Emanuella M. B. Fonseca [a,†], Daniela B. B. Trivella [a,b,‡], Valéria Scorsato [a], Mariana P. Dias [a,§], Natália L. Bazzo [a], Kishore R. Mandapati [a,b], Fábio L. de Oliveira [a,§], Carmen V. Ferreira-Halder [c], Ronaldo A. Pilli [b], Paulo C. M. L. Miranda [b], Ricardo Aparicio [a,*]

[a] Laboratory of Structural Biology and Crystallography, Institute of Chemistry, University of Campinas, CP 6154, 13083-970, Campinas, SP, Brazil
[b] Department of Organic Chemistry, Institute of Chemistry, University of Campinas, CP 6154, CEP 13083-970, Campinas, SP, Brazil
[c] Department of Biochemistry, Institute of Biology, University of Campinas, CEP 13083-862, Campinas, SP, Brazil

ARTICLE INFO

Article history:
Received 17 April 2015
Revised 29 May 2015
Accepted 5 June 2015
Available online 14 June 2015

Keywords:
LMW-PTP
Phosphatase inhibitors
Crystal structure
Enzyme kinetics
Anticancer drugs
Structure-based drug design

ABSTRACT

Low molecular weight protein tyrosine phosphatases (LMW-PTP, EC 3.1.3.48) are a family of single-domain enzymes with molecular weight up to 18 kDa, expressed in different tissues and considered attractive pharmacological targets for cancer chemotherapy. Despite this, few LMW-PTP inhibitors have been described to date, and the structural information on LMW-PTP druggable binding sites is scarce. In this study, a small series of phosphonic acids were designed based on a new crystallographic structure of LMW-PTP complexed with benzylsulfonic acid, determined at 2.1 Å. In silico docking was used as a tool to interpret the structural and enzyme kinetics data, as well as to design new analogs. From the synthesized series, two compounds were found to act as competitive inhibitors, with inhibition constants of 0.124 and 0.047 mM. We also report the 2.4 Å structure of another complex in which LMW-PTP is bound to benzylphosphonic acid, and a structure of apo LMW-PTP determined at 2.3 Å resolution. Although no appreciable conformation changes were observed, in the latter structures, amino acid residues from an expression tag were found bound to a hydrophobic region at the protein surface. This regions is neighbored by positively charged residues, adjacent to the active site pocket, suggesting that this region might be not a mere artefact of crystal contacts but an indication of a possible anchoring region for the natural substrate—which is a phosphorylated protein.

1. Introduction

Protein phosphorylation and dephosphorylation are the main post-translational modifications of proteins in eukaryotic cells.[1] These modifications are catalyzed by protein kinases and phosphatases that modify serine, threonine or tyrosine residues on different proteins, receptors, transcription factors and binding proteins, thus controlling their biological functions. Tyrosine phosphorylation occurs to a much smaller extent than threonine/serine phosphorylation, but it plays a pivotal role in cellular signaling processes.[2–5] The cellular level of the tyrosine phosphorylation is regulated by the opposing activity of protein tyrosine kinases (PTKs) and protein tyrosine phosphatases (PTPs).[6] Therefore, these enzymes control fundamental physiological processes such as cell growth and differentiation, cell cycle, metabolism, cytoskeletal function, and immune response. Accordingly, deregulated activity of PTPs and PTKs is involved in the development of numerous inherited and acquired human diseases such as neurological and cardiovascular disorders, infections, diabetes, cancer, and autoimmunity.[7–9]

Alonso and co-workers[10] demonstrated that human genome contains 107 genes encoding both experimentally verified PTPs and proteins with a domain homologous to the catalytic domain of these PTPs. Among these genes, 81 are predicted to be active protein phosphatases. Based on the primary structure of the

☆ PDB ID codes: 4Z9A, 4Z9B and 4Z99.

* Corresponding author.
E-mail address: aparicio@iqm.unicamp.br (R. Aparicio).
† Present address: Department of Biochemistry, Institute of Biology, University of Campinas, CEP 13083-862, Campinas, SP, Brazil.
‡ Present address: National Center for Research in Energy and Materials, Brazilian Biosciences National Laboratory, 13083-100, Campinas, SP, Brazil.
§ Present address: Institute of Chemistry, University of Campinas, CP 6154, CEP 13083-970, Campinas, SP, Brazil.

http://dx.doi.org/10.1016/j.bmc.2015.06.017
0968-0896/

catalytic domains and the amino acid used in the catalytic reaction, PTPs are subdivided into four evolutionarily distinct classes: I, II, III (cysteine-based PTPs) and IV (aspartate-based PTPs). Despite the three-dimensional structures of the catalytic domains of the cysteine-based PTPs are strikingly similar, they possess different topologies and their regulatory domains vary significantly.[10]

In spite of relatively limited sequence similarity, the most significant feature of the protein tyrosine phosphatase (PTP) superfamily is the conservation of the signature motif CX_5R, which forms the phosphate-binding loop in the active site (known as the P-loop). This structurally conserved arrangement ensures an identical catalytic mechanism where the cysteine and the conserved arginine residues at catalytic site remain in close proximity to hold the phosphate group of the substrate in a position for nucleophilic attack by the cysteine thiol nucleophile.[11]

Low molecular weight protein tyrosine phosphatases (LMW-PTP, EC 3.1.3.48) are a family of enzymes expressed in different tissues with molecular weight up to 18 kDa. They are single-domain enzymes and have been identified in a wide variety of organisms including rat, human, bovine, bacteria, yeast and plants.[12–19] In humans, Class II cysteine-based PTPs are represented by the members of LMW-PTP family (also known as acid phosphatase locus 1, ACP1), which are widely expressed with no particular tissue-specific expression. Four different human LMW-PTP messenger RNA, derived by alternative splicing of a single transcript, have been characterized. Two of them correspond to the classical active isoforms 1 (IF1, PTP*fast*/isoform F or HCPTPA) and 2 (IF2, PTP*slow*/isoform S or HCPTPB).[20] Both isoforms are single polypeptide chains of equal length which display difference only in a short sequence segment that corresponds to amino acid residues 40–73 in the mature protein. However, these isoforms present divergence in their physical chemistry properties, especially with respect to kinetics and consequently physiological functions.[20–23]

In recent years, PTPs have gained considerable attention as important drug targets.[24] However, despite potential inhibitors have been designed, there are challenges in developing successful LMW-PTP inhibitors. Firstly, the low bioavailability and it is very common the observation of reactive oxygen species (ROS) production by reported PTPase inhibitors, with a consequent PTP inhibition occurring by indirect and nonspecific ways.[4,6,10,12,25–27] Since LMW-PTP is proposed as a pharmacological target for cancer chemotherapy,[9,28] it is important to better understand the mechanism and mode of binding of its inhibitors.

LMW-PTP (wild type or mutated) crystallographic structures of a wide range of organisms were reported, most of them presenting ions or other chemical substances contained in the sample buffer, or the synthetic substrate *p*-nitrophenyl phosphate (pNPP).[3,13,29–34] In the case of isoform A human enzyme, structural data are scarce, with two crystal structures of isoform A reported to date, one in which a molecule of 2-(*N*-morpholino)ethanesulfonic acid (MES buffering agent) was observed in the active site (PDB ID 5PNT[3]) and another deposited under the PDB ID 3N8I (unpublished Ref. 35), in which water molecules are observed in the active site pocket and a molecule of 1-naphtylacetic acid (NLA) is bound to a surface region of the protein.

In the present study, a series of compounds was characterized, and three new crystal structures of the isoform A (IF1) of LMW-PTP were determined. These structures comprise one apo LMW-PTP structure and two complexes with small molecule—one with the hydrolysis product of the protease inhibitor PMSF (phenylmethylsulfonyl fluoride) and other in complex with the PMSF analogous benzylphosphonic acid. In both cases, the structures revealed that these compounds bind non-covalently to the LMW-PTP catalytic site, in a very similar fashion as predicted for the natural pTyr substrate, therefore, acting as pTyr mimetic. Further, both in the apo structure and in the complex with benzylphosphonic acid, an unexpected crystallographic site diverse from the known active site is occupied by amino acid residues from the construct expression tag.

2. Results and discussion

2.1. Sulfonic and phosphonic acids as LMW-PTP inhibitors

In the course of the first attempts to crystallize LMW-PTP in our laboratory, we obtained the crystal structure of the enzyme in complex with the hydrolysis product of the protease inhibitor PMSF present in the protein lysis buffer. In an aqueous environment, PMSF can be easily hydrolyzed and the fluorine replaced by a hydroxyl group, yielding benzylsulfonic acid, from now on referred to as PMS (Fig. 1, compound **1**). An additional structure was also available in the literature, in which the active site was occupied by a molecule of 2-(*N*-morpholino)ethanesulfonic acid (MES buffering agent; PDB ID 5PNT3). The presence of a sulfonic acid moiety both in PMS and MES molecules, which can mimic, at some extent, the phosphate group of natural substrates, gave us an initial clue about LMW-PTP and prompted us to design the inhibitors based on phosphonic acids shown in Figure 1, compounds **2** to **7**.

Phosphonic acids are a good choice for the design of phosphatase inhibitors since the replacement of the phenolic oxygen-phosphorus bond in the natural substrate by a non-hydrolysable carbon-phosphorus bond in the phosphonic acid do not alter significantly the geometry or the electric charge distribution, affording appreciable inhibitory activities against these enzymes.[36–38] Benzylphosphonic acid (Fig. 1, compound **2**), in particular, was previously described as a weak inhibitor of phosphatases.[36,37,39–41] Zhang and Van Etten reported that it is a competitive inhibitor of bovine heart acid phosphatase, presenting an apparent inhibition constant of 4.6 mM.[42] Also, it inhibits a human placental alkaline phosphatase (PLAP) and a bovine intestinal 5′-nucleotide phosphodiesterase with inhibition constants of 0.58 mM[36] and 1.4 mM[43], respectively. Benzylphosphonic acid has also been reported as an inhibitor of Yersinia protein tyrosine phosphatase (YopH) and

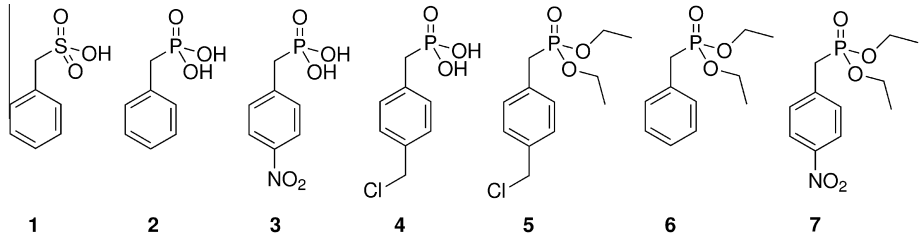

Figure 1. Chemical structure of benzylsulfonic acid (PMS; **1**) and the series of small molecules **2**–**7** designed and synthesized to probe phosphatase inhibitor recognition: benzylphosphonic acid (**2**), 4-nitrobenzylphosphonic acid (**3**), 4-(chloromethyl)benzylphosphonic acid (**4**), diethyl 4-(chloromethyl)benzylphosphonate (**5**), diethyl benzylphosphonate (**6**), diethyl (4-nitrobenzyl)phosphonate (**7**).

PTP1B, with 5 mM and 3 mM as inhibition constants, respectively.[44] In fact, Stebbins et al. proposed that it can be a potential pTyr mimetic bound to the catalytic site of YopH.[45] To our knowledge, this is the first study considering compound **2** as a human LMW-PTP inhibitor.

2.2. Enzyme kinetics and docking studies

The influence of the synthesized compounds on LMW-PTP activity was evaluated by using the classical phosphatases substrate *p*-nitrophenyl phosphate (pNPP) initially in a single concentration activity assay. At a concentration of 2 mM, compounds **3** and **4** were more potent in inhibiting LMW-PTP (Fig. 2A). We thus examined the inhibition mechanism of both compounds to evaluate whether they were indeed acting as a pTyr mimetic. Compounds **3** and **4** act as competitive inhibitors and displayed an inhibitory constant (K_i) of 0.124 and 0.047 mM, respectively (Fig. 2B and C, respectively).

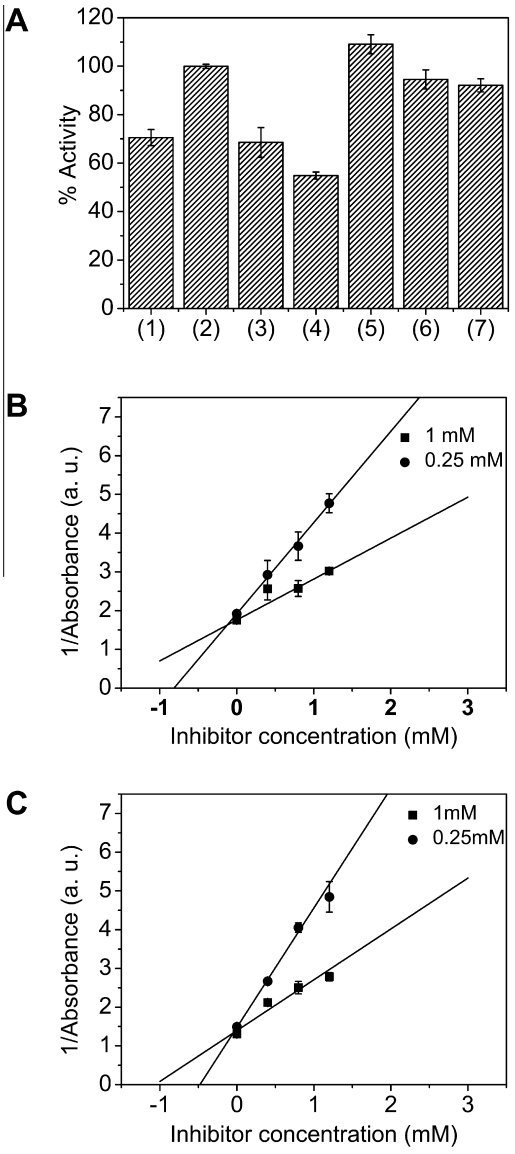

Figure 2. Inhibition assays. (A) Single dose compound screening of phosphatase inhibitors—compound concentration used was 2 mM; (B) Dixon plot for compound **3**; (C) Dixon plot for compound **4**. Compounds **3** and **4** act as competitive inhibitors and displayed an inhibitory constant (K_i) of 0.124 and 0.047 mM, respectively.

When comparing **2**, **3** and **4**, it is reasonable to assume that the substitution at the *para* position led to more effective ligands, probably by favorable interactions at the edge of the active site. Compounds **1** and **2**, despite having almost the same shape, presented different inhibitions toward LMW-PTP although they showed the very same position at the active site of the protein on the complex crystal. It could be a result from the slight difference among conditions used in inhibition assays (pH 5) and crystallization conditions (pH 6.5). Compound **1**, which contains sulfur, is approximately 1000 times more acidic than compound **2** and also has only one acid proton (p*K*a −0.6 for compound **1**, compared to 2.4 for the first proton and 7.8 for the second proton of compound **2**). So, compound **1** is expected to be totally dissociated in any of these pH and always bearing charge −1. Conversely, compound **2** is expected to be 100% monodissociated at pH 5, but 50% monodissociated and 50% fully dissociated at crystallization pH and may have charge −1 or −2 depending on pH value.[46] Thus, considering that P-loop is composed of protonated and positively charged Arg18 and also several N–H peptidic bonds oriented toward to center of the active site (residues Cys12 to Arg18), it is expected that better hydrogen bond acceptors could interact with this environment. Since sulfonate moiety has no bonded hydrogen, it is able to accept a higher number of acidic hydrogen bonds from the active site (P-loop). On the other hand, monodissociated phosphonic acid has only two free oxygen atoms and has a weaker interaction with the active site. According to this rationale, compound **1** would be more effective in inhibiting LMW-PTP, in agreement with the results shown in Fig. 2A.

In order to provide a structural interpretation for the biological assays, molecular modeling studies were done by using an exhaustive rigid-body docking procedure. Our results indicated that compounds **3** and **4** are able to mimic the interaction of the substrate with the catalytic loop. The benzyl group establishes van der Waals interactions with residues Glu50, Asp129 and Tyr131. Figure S1A and B show a two-dimensional representation of the mode of interaction of the compounds with LMW-PTP. Key interactions responsible for the presence of the ligand in that position include hydrogen bonds with amino acid residues Leu13, Gly14, Asn15, Ile16, Cys17, and Arg18. Besides, compound **4** is a benzyl chloride, which is very reactive and can undergo nucleophilic substitution reactions with hydroxyl, thiol and amine present in the side chain of the protein.

Compounds **5**, **6** and **7**, on the other hand, have no shape complementarity with the active site, since the ethyl group forming esters are very bulky compared to the phosphate moiety. Moreover, these small alkyl substituents decrease the possibility of forming hydrogen bond or ionic interactions with the P-loop residues of LMW-PTP in the bottom of the active site. According to our docking results, these ester compounds are accommodated in the opposite direction when compared to **1** or **2**, as illustrated in Figure S2. In addition, van der Waals interactions in the adjacent region (residues Tyr49, Tyr132) of the active site were observed with the ester groups.

2.3. New crystal structures of LMW-PTP

Human LMW-PTP consists of a four-stranded central parallel β-sheet with flanking α-helices on both sides. The active site consists of a loop located between β-1 and α-1 (Fig. S4), which contains the consensus sequence motif CX_5R (CLGNICR in the present case). The complete amino acid sequence of the construct used in this study is shown in Fig. S3. The protein construction included the His-tag sequence MGSSHHHHHHSSGLVP**RG**SHMEF. The His-tag cleavage by thrombin occurs between the residues arginine and glycine

(residues −7 and −6 marked in bold). For this reason, a remaining polypeptide (residues −6 to −1, underlined), the expression tag, remains bound to the protein N-terminal.

LMW-PTP crystals contain a single molecule in the asymmetric unit (ASU), in a molecular arrangement in which the active site is unreachable through solvent channels due to an occlusion resulting from protein–protein crystal-packing contacts. This feature limited the use of soaking to obtain complexes once the access of small molecules to the active site is restricted. In spite of numerous attempts, we did not succeed in obtaining another crystal form of LMW-PTP. Therefore, attempts to obtain crystal structures of LMW-PTP in complex with the compounds **2**–**7** were done by co-crystallization.

Data collection and refinement statistics for complexes with **1** and **2** (PDB ligand codes PMS and B85, respectively) in addition to an apo structure, are summarized in Table 1. The expression tag interacts with a neighbor molecule both in the complex with **2** and in the apo LMW-PTP structure, suggesting the existence of a secondary binding site, as discussed in further detail below.

The refined model of LMW-PTP in complex with **1** contains 154 amino acid residues. The N-terminal was flexible, and electron density was observed starting from residue Ala4 (Fig. S3). PMS resembles a phosphorylated tyrosine (pTyr), which is the natural substrate of PTPases. Not surprisingly, as a pTyr mimetic, the ligand is recognized by the PTPase catalytic motif CX_5R. The oxygen atoms of PMS establish several interactions with the main chain nitrogen of the residues Leu13, Gly14, Asn15, Ile16, Cys17 and Arg18. Moreover, hydrogen bonds with Nε and NH2 atoms from Arg18 side chain were also observed. The benzyl ring is well accommodated near Tyr131 side chain at the entrance of LMW-PTP catalytic site (Fig. 3A), with van der Waals interactions occurring with residues Cys12, Leu13, Ile16, Glu50, Asp129 and Tyr131. A glycerol molecule, from cryoprotectant solution, was modeled and is stabilized by hydrogen bond interactions with Glu93 and Arg97. Interestingly, among the three structures, only in the PMS complex, the side chain of Arg97 adopts a different conformation. The same conformation was previously observed in the structure reported as PDB ID 5PNT[3] although without any apparent interaction which would explain it. On the other hand, the conformation adopted by Arg97 in the other two structures (apo LMW-PTP and LMW-PTP:**2**) was already observed in PDB ID 3N8I,[35] and can be explained by crystal contacts with neighboring molecules (Fig. 3).

Table 1
Data collection and refinement statistics[a]

	Structure		
	LMW-PTP:**1**	LMW-PTP:**2**	apo LMW-PTP
PDB ID	4Z9A	4Z9B	4Z99
Data collection statistics			
Space group	$P2_12_12_1$	$P2_12_12_1$	$P2_12_12_1$
Solvent content (%)	50.0	47.6	50.0
Cell dimensions (Å):			
a	32.75	32.09	32.67
b	55.23	54.29	54.16
c	97.80	97.47	100.05
Resolution range (Å)	28.07–2.10	27.88–2.41	36.75–2.30
Last resolution shell (Å)	2.21–2.10	2.40–2.45	2.30–2.35
Multiplicity	4.0 (4.0)	11.84 (11.58)	8.57 (7.94)
R_{sym} (%)	8.5 (50.8)	14.55 (56.18)	22.62 (62.10)
$\langle I/\sigma(I)\rangle$	9.2 (2.2)	16.34 (2.94)	7.43 (2.0)
Refinement statistics			
No. of reflections in refinement	9846	6641	7967
Completeness (%)	97.59	99.26	99.68
No. of reflections used for R_{free} (5%)	796	325	385
R-factor—all reflections (%)	18.21	21.81	19.43
R-factor—excluding test set (%)	17.80	21.41	19.02
R-free (%)	23.47	30.10	28.59
protein atoms	1245	1260	1294
water molecules	88	69	122
Ligand atoms	27	11	0
Average B-factor for protein atoms ($Å^2$)	41.76	34.90	25.11
RMS deviations from ideality:			
Bond lengths (Å)	0.014	0.013	0.013
Bond angles (°)	1.665	1.566	1.490
Ramachandran analysis			
Favoured regions (%)	96.0	96.0	98.0
Allowed regions (%)	4.0	4.0	2.0
Outlier regions (%)	0.0	0.0	0.0

[a] Values in parentheses refer to the last resolution shell.

In the case of LMW-PTP in complex with **2**, a total of 157 amino acid residues could be modeled. In this experiment, crystals were produced from protein expressed and purified in the absence of PMSF to prevent an eventual interaction between the enzyme and its hydrolysis product (PMS), as stated in Section 4.2, thus allowing us to confirm compound **2** as the unique ligand candidate to be present in solution. In the final structure, a non-contiguous N-terminal was built, starting from the amino acid His-4 which belongs to the expression tag included in the construct (Fig. S3). No electron density was visible for residues Met0 to Ala4. In spite of its negligible inhibitory activity, concentration of **2** in the crystallization media was high enough to provide full occupancy of the ligand atoms, which were found at the active site pocket (Fig. 3B). Compound **2** exhibited virtually the same mode of binding observed in the complex with PMS. In summary, the oxygen atoms of the phosphonate group were located at the bottom of the active site, sitting on the phosphate binding pocket and forming multiple hydrogen bonds with the nitrogen atoms of the active site loop backbone, and NH2 and Nε atoms from Arg18 side chain. Moreover, the edge is lined by the hydrophobic residues Leu13, Ile16 and Tyr131, which form a suitable interaction surface that can accommodate the benzyl group, and may interact with the bound ligand (Fig. 3B).

In the apo structure, reliable electron density maps were found for all of the 164 amino acid residues, comprising the whole construct of LMW-PTP, including the entire expression tag. Despite the presence of compound **3** in the crystallization solution (Section 4.4), no ligand is observed at the active site, which is occupied by water molecules linked together by a hydrogen bond network within the active site (Fig. 3C). Interestingly, the oxygen atoms belonging to three of these water molecules are found at almost the same position as the oxygen atoms of the phosphonate group from compound **2** in the structure LMW-PTP:**2** (Fig. S5).

Except for the N-terminal, no significant conformational changes are observed in the protein chain when comparing the three structures (average RMSD for common residues less than 1 Å). Both ligands **1** and **2** are well-ordered and the atom positions fully occupied. Their modes of binding are nearly identical, which is not surprising in view of their structural similarity and volume (Fig. 1). Moreover, no structural changes in the active site environment were found to explain the difference observed in their inhibition effect nor apparent conformational changes in this region are observed when comparing the structures reported here to the structures 5PNT and 3N8I available at the PDB. The structural similarity reveals that the presence of these compounds, regardless their nature, cannot induce appreciable conformational changes in the protein structure. All of the structures (both previously reported and those described in the present work) share a common crystal packing, belonging to a same space group ($P2_12_12_1$), with similar solvent content (~50%), cell dimensions and a single molecule in the crystal ASU. Thus, we can argue that the differences

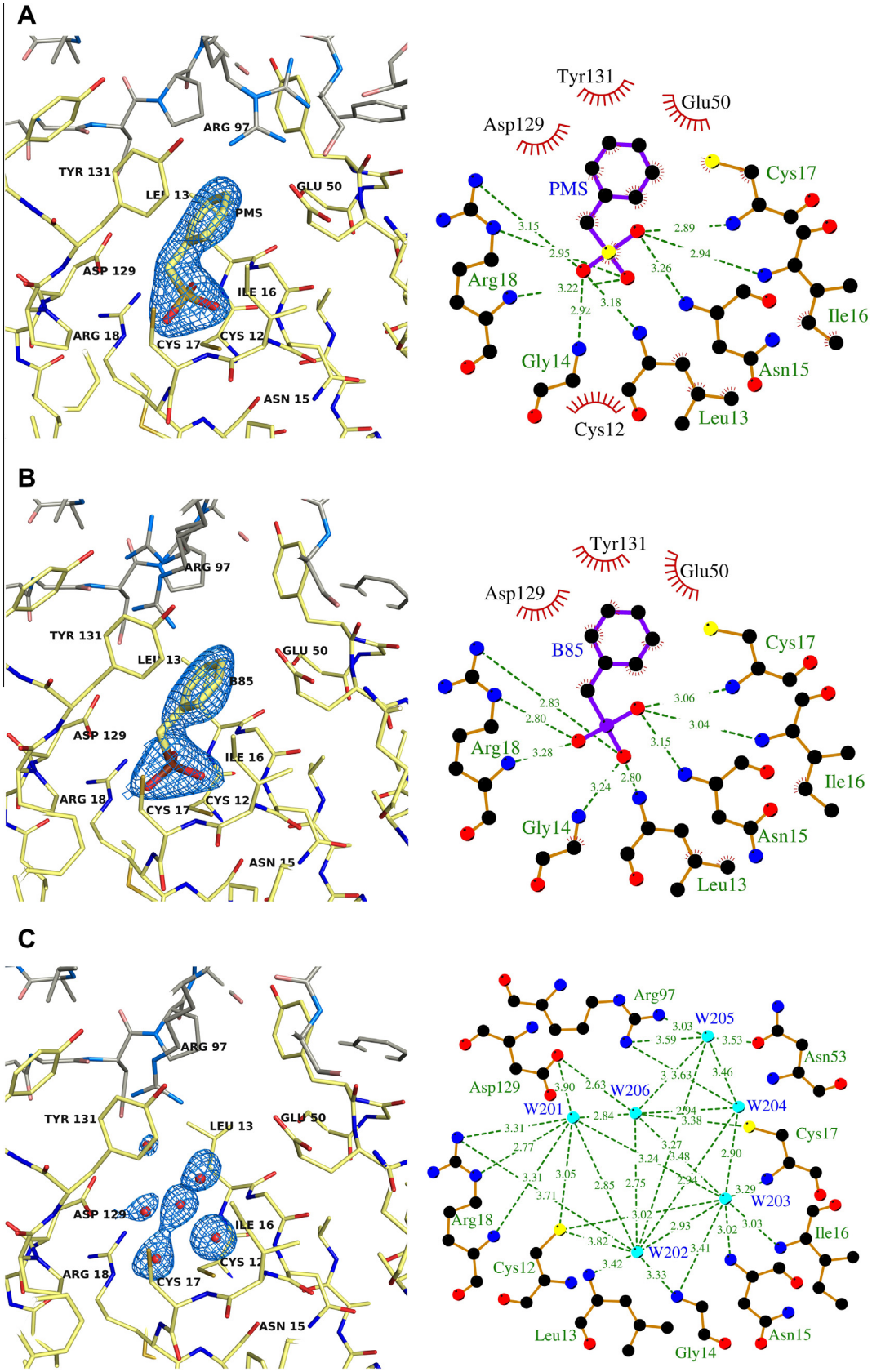

Figure 3. Crystal structures of human LMW-PTP showing the active site region (left panel) and corresponding chemical interactions (right panel). Electron density maps ($2F_{obs} - F_{calc}$) are shown at 1.0 σ (blue) for LMW-PTP:**1** (A), LMW-PTP:**2** (B) and apo LMW-PTP (C). Schematic diagram created by using LIGPLOT+.[73,74] In the left panel, amino acid residues belonging to symmetry-related molecules have carbon atoms shown in grey, and water molecules far from the active site pocket have been omitted for clarity. In the right panel, green dotted lines indicate hydrogen bonds within the given lengths. Hydrophobic interactions are represented as red eyelashes around the protein residue names and ligand atoms. In (C), water molecules are shown as spheres in cyan.

observed in the inhibiting ability of each compound is probably due to the chemical nature of intermolecular interactions between the ligand and the phosphatase, as anticipated in Section 2.2. In other words, the difference in their inhibition effect is due the different state of protonation of the compounds.

2.3.1. An unexpected binding site

Both crystal structures of LMW-PTP in the apo form and in complex with ligand **2** feature an unexpected binding site occupied by amino acid residues Glu-2 and Phe-1 from the polypeptide GSHMEF belonging to the expression tag (amino acids −6 to −1; Fig. S3) of a molecule related by crystallographic symmetry. No significant RMSD was found for the common residues of the expression tag modeled in both structures.

This site was previously described as a secondary binding site, according to the PDB structure 3N8I,[35] in which it is occupied by a molecule of the compound 1-naphtylacetic acid (NLA). The superposition shown in Figure 4C reveal a striking chemical similarity between the ligand NLA and the amino acid residues Glu-Phe from the expression tag in our structures. Interestingly, in both cases an aromatic ring and a carboxylic acid moiety are observed. In our apo structure (Fig. 4A) and in the complex LMW-PTP:**2** (Fig. 4B), amino acids Glu-Phe interacts in a cleft between α-3 and α-4 close to the active site responsible for the catalysis, in a region formed by a hydrophobic pocket, with the presence of residues Thr78 and Phe82, surrounded by the polar residues Gln76, Lys79, Arg101, Lys102, Gln105. In the complex LMW-PTP:**1**, a sulfate ion is found in the same region as the carboxylic acid of Glu-2 (Fig. S6).

To better understand the chemical nature of the interactions and mode of binding of the amino acids Glu-Phe, all of the residues (including those from symmetric molecules) within a sphere of radius 10 Å centered on this region were taken into account in order for calculation and visual inspection of chemical bonds. Our analysis of the interaction between the amino acids Glu-Phe and all of the residues contained in the constructed spherical region, revealed that Glu-2 and Phe-1 are stabilized by chemical contacts provided by contacts within a single protein molecule, without participation of symmetry-related molecules (Fig. 4C, molecule colored in yellow). The side chain of the tag residue Phe-1 was well accommodated within the hydrophobic pocket, interacting through van der Waals forces. At the same time, the carboxylic acid of Glu-2 forms hydrogen bonds with the side chain of the residues Arg101, Lys102 and Gln105 (Fig. 4D). In addition to the chemical interactions observed, it is worth noting that although clear electron density maps were observed for segment Glu-Phe, which is well-ordered both in apo structure and in the complex with **2**, a non-contiguous N-terminal was modeled in the structure LMW-PTP:**2**, as mentioned above, with no electron density observed for the residues Met0 to Ala4. Surprisingly, in spite of the disorder of this linker, the beginning of the expression tag is firmly grasped to the protein surface (Fig. 4B). Whether this feature is an artefact of crystal contacts has no obvious answer.

Conceivably, both features seems to be an indication that this region has a singular affinity for peptides. If such hypothesis is correct, a possible biological role for this region might be to act as an anchor site for the biological substrate of this PTP. In this regard, it is noteworthy that residues Gln76, Thr78 and Phe82, directly involved in the binding of the amino acids Glu-Phe, are highly conserved across homologous sequences of vertebrates, as calculated by the ConSurf method[47–50] (Fig. S4), which might be an indication of their importance for protein function. It is worth to mention that, in the case of another phosphatase, CDC25B, residues located far from the active site have been reported as involved in substrate recognition[51] and recent results proved that targeting the enzyme at this region disrupt protein-protein interactions.[52]

3. Conclusion

In this study, a small series of molecular fragments have been designed and assayed against human LMW-PTP. Three inhibitors were identified, two of them acting by a competitive mechanism. In spite of the weak inhibition observed, the fragments have an optimized binding mode and could be used as potential starting points for designing more potent LMW-PTP inhibitors. Structures of LMW-PTP reported in the present work feature a region distinct from the active site, apparently propense to bind amino acid residues. More experiments are necessary to determine whether this additional site is important for LMW-PTP function and how it could be explored to modulate protein action.

4. Material and methods

4.1. Chemistry

The synthesis of alkyl phosphonates was achieved according to previously published procedures utilizing the Arbuzov reaction of substituted benzyl halides with triethyl- or trimethylphosphite.[39] Phosphonic acids syntheses were performed by concentrated chloridric acid or chlorotrimethylsilane/sodium iodide mediated hydrolysis of the intermediate esters.[53,54] All solvents were treated according to procedures outlined by Armarego and Chai.[55] Organic layers were dried over anhydrous Na_2SO_4. Concentration under reduced pressure was performed by rotary evaporation (~30 torr) at 20–40 °C. Flash column chromatography was performed as described elsewhere,[56] employing Merck silica gel 60 (spherical, diameter range 40–100 μm). Analytical thin-layer chromatography (TLC) was performed on Merck analytical plates pre-coated with silica gel 60 F254 (0.25 mM thick). TLC plates were visualized by exposure to ultraviolet light (UV) and/or exposure to phosphomolybdic acid solution followed by brief heating on a hot plate. Infrared (IR) spectra were recorded on a Therm Scientific Nicolet iS5 Fourier transform spectrophotometer and are reported in wavenumbers (cm^{-1}). Proton nuclear magnetic resonance (^1H NMR) spectra and carbon nuclear magnetic resonance (^{13}C NMR) spectra were determined on Bruker Avance (^1H NMR: 250 or 400 MHz, and ^{13}C NMR: 62.5 or 100 MHz) instruments. Chemical shifts are reported in parts per million (δ scale) downfield from tetramethylsilane as the internal standard, with coupling constants expressed in hertz (Hz). The following abbreviations were used for spin multiplicity: s = singlet, d = doublet, t = triplet, m = multiplet, br = broad. High resolution mass spectrometry (HRMS) analyses were carried out in a Waters Micromass-Q-TOF (ESI/APCI, negative mode).

4.1.1. Diethyl benzylphosphonate (6)

Triethylphosphite[57,58] (0.5 mL, 0.0029 mmol) was added to benzyl bromide (500 mg, 0.0029 mmol) in a round bottom flask under inert atmosphere and stirred at 135 °C for 12 h. The crude reaction mixture was purified by column chromatography silica gel with AcOEt/hexanes (50:50, rf = 0.44) as eluent to yield (**6**) as a colorless oil (72%).

4.1.2. Benzylphosphonic acid (2)

Diethyl benzylphosphonate[59] (**6**, 500 mg, 0.0022 mmol) was treated with conc. HCl (8 mL) and stirred under reflux for 24 h in a round bottom flask. The reaction mixture was cooled to room temperature and the resulting precipitate was filtered, washed with cold water and dried in vacuum. Benzylphosphonic acid (**2**) was isolated in 70% yield (mp 160–163 °C).[60] ^1H NMR (DMSO-d_6, 250 MHz): δ_H (ppm) 7.30–7.17 (m, 5H), 2.94 (d, br, $^2J(^1H–^{31}P)$ = 21.4 Hz, 2H); ^{13}C NMR (DMSO-d_6, 62.5 MHz): δ_C (ppm) 35.4 (d, br,

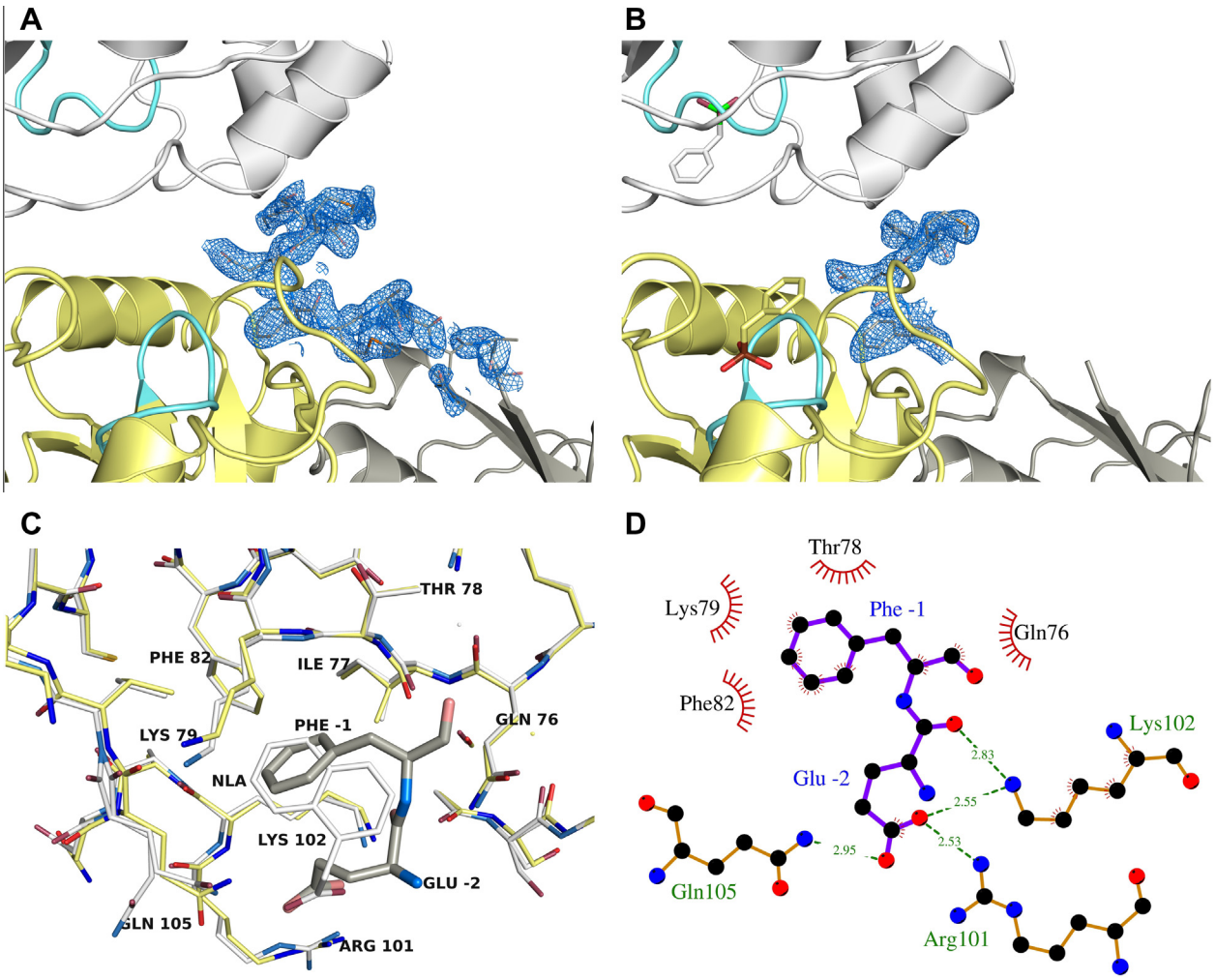

Figure 4. Crystal structure of apo LMW-PTP (A) and LMW-PTP:**2** (B), exhibiting clearly defined electron density maps ($2F_{obs} - F_{calc}$ shown at 1.0 σ, colored in blue) for amino-terminal residues His-4–Phe-1 and Gly-6–Met0, respectively. Crystallography symmetry mates of the single molecule contained in the crystal ASU (colored in yellow) are shown in grey. The active site region is colored in cyan. Panel (C) presents a superposition of the structures LMW-PTP:**2** and PDB ID 3N8I, showing the region in which both the amino acids Glu-2, Phe-1 and the compound NLA interact with the protein. In (A), (B) and (C), water molecules have been removed for clarity. Panel (D) shows the corresponding chemical interactions observed in the complex LMW-PTP:**2**. Schematic diagram created with LIGPLOT+.[73,74] Green dotted lines indicate hydrogen bonds within the given lengths. Hydrophobic interactions are represented as red eyelashes around the protein residue names and ligand atoms.

$^{1}J(^{13}C–^{31}P)$ = 131.4 Hz), 126.0 (d, $^{5}J(^{13}C–^{31}P)$ = 3.0 Hz), 128.0 (d, $^{4}J(^{13}C–^{31}P)$ = 2.5 Hz), 129.8 (d, $^{3}J(^{13}C–^{31}P)$ = 6.5 Hz), 134.2 (d, $^{2}J(^{13}C–^{31}P)$ = 8.6 Hz); ^{31}P NMR (DMSO-d_6, 101.0 MHz): δ 20.9 (s); IR (ATR) ν_{max} (cm^{-1}) = 1491, 1458, 1260, 1074, 989, 942, 782, 701, 693; HRMS (ESI-TOF) *m/z*: calcd. for $C_7H_9O_3P$ $[M–H]^-$ = 171.0211; observed $[M–H]^-$ = 171.0201.

4.1.3. 4-Nitrobenzylphosphonic acid (3)

Diethyl benzylphosphonate[61,62] (**6**, 500 mg, 0.0022 mmol) was treated with a 1:1 mixture of conc. H_2SO_4 and conc. HNO_3 (5 mL) at 0 °C in a round bottom flask. The reaction mixture was stirred at 0 °C for 40 min and then treated with ice/cold water. The crude reaction mixture was extracted with ethyl acetate and then the organic layer washed with brine, dried with sodium sulfate, and concentrated under reduced pressure. The residue was purified by column chromatography in silica gel with AcOEt/hexanes (50:50) to yield diethyl 4-nitrobenzylphosphonate **7** as a yellowish oil. This intermediate was hydrolyzed with conc. HCl as described in section 4.1.2 furnishing 4-nitrobenzylphosphonic acid **3** as light yellow crystals in 60% overall yield (mp 224–227 °C).[61] ^{1}H NMR (CD_3OD, 250 MHz): δ_H (ppm) 8.04 (d, *J* = 8.3 Hz, 2H), 7.41 (d, *J* = 8.3 Hz, 2H), 3.14 (d, br, $^{2}J(^{1}H–^{31}P)$ 22.0 Hz, 2H); ^{13}C NMR (CD_3OD, 62.5 MHz): δ_C (ppm) 36.1 (d, br, $^{1}J(^{13}C–^{31}P)$ = 132.5 Hz), 124.5 (d, $^{4}J(^{13}C–^{31}P)$ = 2.9 Hz), 132.1 (d, $^{3}J(^{13}C–^{31}P)$ = 6.1 Hz), 143.0 (d, $^{2}J(^{13}C–^{31}P)$ = 9.2 Hz), 148.3 (d, $^{5}J(^{13}C–^{31}P)$ = 3.6 Hz); ^{31}P NMR (CD_3OD, 101.0 MHz): δ 21.9 (s); IR (ATR) ν_{max} (cm^{-1}) = 1609, 1599, 1519, 1491, 1419, 1403, 1344, 1267, 1180, 1153, 1107, 1073, 984, 969, 949, 860, 823, 771, 697; HRMS (ESI-TOF) *m/z*: calcd. for C_7H8NO_5P $[M–H]^-$ = 216.0062; observed $[M–H]^-$ = 216.0052.

4.1.4. 4-(Chloromethyl)benzylphosphonic acid (4)

A mixture of α,α′-dichloro-*p*-xylene (500 mg, 0.0028 mmol) and triethylphosphite (0.23 mL, 0.0014 mmol) was refluxed at 125 °C for 16 h in a round bottom flask under inert atmosphere.[54,63] The crude reaction mixture was purified by column chromatography in silica gel with AcOEt/hexanes (50:50) to furnish diethyl 4-(chloromethyl)benzylphosphonate (**5**) as a colorless oil. Compound **5** (370 mg, 0.0013 mmol) was treated with TMSCl (0.50 mL, 0.0039 mmol) in dry acetonitrile at 0 °C under N_2 atmosphere. The reaction mixture was stirred for 6 h at room temperature and afterward the solvent was removed under reduced

pressure. The crude reaction mixture was treated with methanol (10 mL), stirred at room temperature for 1 h, and then the solvent was removed under vacuum. After that, the residue was treated with water and stirred for additional 15 min. The white solid was filtered off, washed with cold water, and then dried under vacuum to furnish 4-(chloromethyl)benzylphosphonic acid (**4**) in 30% overall yield (mp 151–153 °C). ^{1}H NMR (CD_3OD, 400 MHz): δ_H (ppm) 7.14 (s, 4H), 4.41 (s, 2H, $-CH_2Cl$), 2.93 (d, $^{2}J(^{1}H-^{31}P)$ = 22.1 Hz, 2H); ^{13}C NMR (CD_3OD, 100.0 MHz): δ_C (ppm) 35.8 (d, br, $^{1}J(^{13}C-^{31}P)$ = 136.0 Hz), 46.8 ($-CH_2Cl$), 129.9, 131.4 (d, $^{3}J(^{13}C-^{31}P)$ = 5.7 Hz), 135.0 (d, $^{2}J(^{13}C-^{31}P)$ = 7.5 Hz), 137.8; ^{31}P NMR (CD_3OD, 202.0 MHz): δ 23.9 (s); IR (ATR) ν_{max} (cm^{-1}) = 1515, 1420, 1409, 1261, 1227, 1109, 1092, 992, 970, 954, 941, 844, 800, 757, 713, 617; HRMS (ESI-TOF) *m/z*: calcd. for $C_8H_{10}ClO_3P$ $[M-H]^-$ = 218.9978, $[M-H+2]^-$ = 220.9951; observed $[M-H]^-$ = 218.9985, $[M-H+2]^-$ = 220.9961.

4.2. Expression and purification

LMW-PTP clone was commercially acquired from GenScript (GenScript USA Inc., Piscataway, New Jersey, USA). The coding sequences were subcloned into pET28a vector, in which protein expression is regulated by regulators T7 promoter and Lac operon. A 6x His-tag was added to the N-terminal portion of the protein to facilitate subsequent purification. Two different expression protocols were used, either in the presence or absence of the protease inhibitor PMSF, as described below.

In Protocol I, cells of *Escherichia coli* BL21 (DE3) transformed with the vector pET28a, were grown in LB medium at 37 °C for three hours (180 rpm). Protein expression was induced by adding 0.5 mM of IPTG, with incubation proceeding for an additional 5 h at 15 °C. After centrifugation, the cells were recovered and disrupted in a lyse buffer (1 M Tris pH 7.5, 250 mM NaCl, 1% (v/v) Triton X-100, 5 mM DTT, 1 mM EDTA and 5 mM imidazole) containing 1 mg mL^{-1} of lysozyme. After 30 min, the solution was sonicated and centrifuged at 4 °C, with a RCF equal to 18000*g*, for 20 min. The protein was purified from the supernatant by immobilized metal affinity chromatography, using nickel resin (Ni Seph 6 Fast Flow, GE, LifeSciences), by applying an imidazole gradient (20–500 mM). The His-tag was cleaved with thrombin (Sigma–Aldrich) 0.1 U mg^{-1}. All of the buffer solutions also contained 0.1 mM PMSF. In Protocol II, cells of *E. coli* BL21 (DE3) transformed with pET28a were grown in LB medium at 37 °C, overnight, in a shaker at 180 rpm. Protein expression occurred in an auto-inducing medium prepared by adding 0.5 mL of 1 M $MgSO_4$, 10 mL of 50x 5052 solution (25% glycerol, 2.5% glucose, and 10% α-lactose monohydrate) and 25 mL of 20x NPS solution (1 M Na_2HPO_4, 1 M KH_2PO_4, 0.5 M $(NH_4)_2SO_4$), to a volume of 500 mL of ZY medium. The auto-inducing medium was then kept at 30 °C for 20 hours in a shaker at 180 rpm. Following centrifugation, cells were recovered and disrupted in a lyse buffer (1 M Tris pH 7.5, 250 mM NaCl, 1% (v/v) Triton X-100, 5 mM DTT, 1 mM EDTA and 5 mM imidazole) containing 1 mg mL^{-1} of lysozyme. After 30 min, the solution was sonicated and centrifuged at 4 °C, RCF of 18000*g*, for 20 min. Protein purification was done as described in Protocol I, except for the absence of PMSF in all of the buffer solutions.

4.3. Enzyme kinetics assays

4.3.1. Single dose compound screening

The reaction mixture (100 μL) containing 100 mM sodium acetate buffer (pH 5.0), 10 mM pNPP, and enzyme was incubated for 10 min at 37 °C, and then stopped by the addition of 100 μL of 1 M NaOH. The relative absorbance was read at 405 nm. To evaluate the effect of a potential inhibitor on PTP activity, the compound was dissolved in DMSO, except PMSF (alcoholic solution), to a final concentration in the reaction medium equal to 2 mM. PTP activity in the presence of DMSO was considered as 100%. All assays were conducted in triplicate.

4.3.2. Determination of inhibition constant

The inhibition constants were determined from Dixon plots.[64] The enzyme activity was determined in the presence of two constant concentrations of pNPP and varying concentrations of inhibitors. The K_i values were obtained from the intersection of the curves read of from the abscissa axis. Data were normalized to a DMSO control and all the assays were conducted in triplicate.

4.4. Protein crystallization, structure determination and analysis

LMW-PTP crystals grow within 1–2 weeks at 18 °C, using the hanging drop method. Complexes with **1** and **2** were obtained by co-crystallization. In the case of LMW-PTP:**1**, a reservoir solution (400 μL) consisting of 26% (w/v) PEG 5000 (Aldrich), 0.2 M ammonium sulfate, 0.2 M MES buffer (Aldrich) pH 6.5, was mixed in equal amounts (1 μL:1 μL) with a solution of LMW-PTP at a concentration of 10 mg mL^{-1} in a buffer containing 10 mM Tris pH 8.0, 25 mM NaCl, 3 mM DTT, 0.2 mM EDTA. The hydrolysis product (**1**; Fig. 1) of the protease inhibitor PMSF, used during protein purification, remained bound to the active site, without further addition of PMSF to the crystallization buffer.

Since the presence of the buffering agent MES would displace LMW-PTP ligands and there was hope in finding new crystal packing, we searched for new LMW-PTP crystallization conditions. Crystallization set ups were conducted automatically with the Honey Bee robot at the Brazilian Biosciences National Laboratory (RoboLab LNBio—CNPEM). A new LMW-PTP crystallization condition was found, in the presence of MMT buffer (malic acid, MES and Tris buffers), but in the same space group. Based on this initial condition we refined the solutions and found good LMW-PTP crystals in the conditions described below, replacing MES by the inhibitors compounds.

To crystallize the complex LMW-PTP:**2**, a reservoir solution (300 μL) containing 32% (w/v) PEG 5000 (Aldrich), 0.1 M malic acid (Aldrich):Tris (Sigma), molar ratio 1:2, pH 7.0 was mixed in equal amounts (1 μL:1 μL) with a solution of LMW-PTP at a concentration of 9 mg mL^{-1}, in the same protein buffer. Compound **2** was added to the protein solution, at a concentration of 1.45 mM, immediately before the set up of the crystallization assays.

The structure of the apo form of LMW-PTP was determined from a crystal grown in a drop prepared by mixing 1 μL of a reservoir solution (300 μL) containing 27% (w/v) PEG 2000 (Fluka), 0.1 M malic acid (Aldrich):Tris (Sigma), molar ratio 1:2, pH 7.0, to 1 μL of a protein solution (at 9 mg mL^{-1}) consisting of 10 mM Tris pH 7.5, 25 mM NaCl, 3 mM DTT, 0.2 mM EDTA. This crystal was obtained during screening of potential LMW-PTP complexes. Thus, it is worth noting that, even though no ligand is observed in the final structure, the crystallization drop contained ligand **3** (Fig. 1) at a concentration of 1.45 mM before equilibration of the crystallization drops.

For both LMW-PTP:**2** and apo LMW-PTP, X-ray diffraction experiments were performed with a Bruker Kappa APEX II Duo diffractometer, equipped with an Incoatec IμS Quazar MX microfocus source providing Cu Kα radiation (λ = 1.5418 Å). The exposure time was 75 s, with an oscillation range of 0.5° per frame, and a crystal-to-detector distance equal 50 mM or 60 mM for the apo form and the complex, respectively. To prevent radiation damage, crystals were soaked in a cryoprotectant solution consisting of crystallization reservoir solution supplemented with 15% (v/v) glycerol, and flash-cooled in a nitrogen-gas stream at −173 °C (Oxford Cryosystems, 700 Series). In both cases, data reduction

(integration and scaling) was performed with the APEX II software suite (Bruker AXS Inc., Madison, Wisconsin, USA). Diffraction images for the complex of LMW-PTP:**1** were collected at the beamline W01B-MX2 of the Laboratório Nacional de Luz Síncrotron (LNLS—Campinas, SP, Brazil), using a MAR Mosaic CCD 225 detector, by the oscillation method with 1.0° oscillation per frame. A total of 115 images were collected with a crystal-to-detector distance of 121.568 mM, at a X-ray wavelength of 1.459 Å and a 90 s exposure time. Data were integrated with *MOSFLM* and scaled using *SCALA*.[65]

The phase problem was solved by the molecular replacement method, using the program PHASER[66] and PDB ID 5PNT[3] as the search model. Structure refinement was carried out with the program REFMAC[65,67] and COOT[68] for graphical analysis and model building. In the course of structure refinement, occupancies of selected atoms were refined with PHENIX.[69] Ligand RMSD values were calculated with Chimera.[70] RMSD for protein chains were obtained with the VMD package.[71] The quality of the structures was evaluated through the wwPDB Deposition Tool[72] and COOT internal routines. Intermolecular interactions were assessed using the program LIGPLOT,[73,74] also used for figures composition. Figures were prepared using PyMol (The PyMOL Molecular Graphics System, Schrödinger, LLC),[75] which have also been used for structural analysis. Structures superposition were obtained with CEAlign[76] implemented as a PyMOL plugin. The coordinates of the new structures LMW-PTP:**1**, LMW-PTP:**2** and apo LMW-PTP, have been deposited with the Protein Data Bank with accession codes 4Z9A, 4Z9B and 4Z99, respectively.

4.5. Docking studies

Docking studies were performed with FRED77 (FRED version 2.2.5, OpenEye Scientific Software, Santa Fe, NM; http://www.eyesopen.com), using the Chemgauss3[77] scoring function. The crystal structure of the complex LMW-PTP:**1** was used as the receptor and prepared with FRED_Receptor using the ligand **1** as a reference to determine the active site location. This input was sufficient to predict a crystallographic pose of the ligand present at the active site, resulting in a RMSD value (for the ligand atoms) near 2 Å in the re-docking experiment. A conformational database of compounds **3**–**7** was prepared using Makefraglib and OMEGA[78,79] (OMEGA version 2.4.3, OpenEye Scientific Software, Santa Fe, NM; http://www.eyesopen.com). In order to not restrict the pose selection, no constraints were used. The best ranked pose for each compound was retained and analyzed.

Acknowledgements

The authors acknowledge Fundação de Amparo à Pesquisa do Estado de São Paulo (FAPESP Grants 09/51602-5, 10/17544-5, 11/15792-4, 11/03054-9), Coordenação de Aperfeiçoamento de Pessoal de Nível Superior (CAPES) and Conselho Nacional de Desenvolvimento Científico e Tecnológico (CNPq) for financial support. R.A. is the recipient of a research grant from CNPq. K.R.M. was supported by a TWAS/CNPq PhD grant (190655/2011-9). We gratefully acknowledge the Laboratório Nacional de Luz Síncrotron (LNLS) for W01B-MX2 beamline time and the Laboratório Nacional de Biociências for the use of the crystallization facility (RoboLab). We also thank OpenEye Scientific Software Inc. for providing an academic license.

Supplementary data

Supplementary data associated with this article can be found, in the online version, at http://dx.doi.org/10.1016/j.bmc.2015.06.017.

References and notes

1. Hunter, T. *Cell* **1987**, *50*, 823.
2. Zhang, Z. Y. *Crit. Rev. Biochem. Mol. Biol.* **1998**, *33*, 1.
3. Zhang, M.; Stauffacher, C. V.; Lin, D.; Van Etten, R. L. *J. Biol. Chem.* **1998**, *273*, 21714.
4. Ramponi, G.; Stefani, M. *Biochim. Biophys. Acta, Protein Struct. Mol. Enzymol.* **1997**, *1341*, 137.
5. Hunter, T. *Cell* **1995**, *80*, 225.
6. Maccari, R.; OttanÃ, R.; Ciurleo, R.; Paoli, P.; Manao, G.; Camici, G.; Laggner, C.; Langer, T. *ChemMedChem* **2009**, *4*, 957.
7. Ferreira, C. V.; Justo, G. Z.; Souza, A. C. S.; Queiroz, K. C. S.; Zambuzzi, W. F.; Aoyama, H.; Peppelenbosch, M. P. *Biochimie* **1859**, *2006*, 88.
8. Andersen, J. N.; Jansen, P. G.; Echwald, S. M.; Mortensen, O. H.; Fukada, T.; Del Vecchio, R.; Tonks, N. K.; MÃller, N. P. H. *FASEB J.* **2004**, *18*, 8.
9. Ferreira, P. A.; Ruela-de Sousa, R. R.; Queiroz, K. C. S.; Souza, A. C. S.; Milani, R.; Pilli, R. A.; Peppelenbosch, M. P.; den Hertog, J.; Ferreira, C. V. *PLoS One* **2012**, *7*, e44312.
10. Alonso, A.; Sasin, J.; Bottini, N.; Friedberg, I.; Friedberg, I.; Osterman, A.; Godzik, A.; Hunter, T.; Dixon, J.; Mustelin, T. *Cell* **2004**, *117*, 699.
11. Tabernero, L.; Aricescu, A. R.; Jones, E. Y.; Szedlacsek, S. E. *FEBS J.* **2008**, *275*, 867.
12. Alho, I.; Costa, L.; Bicho, M.; Coelho, C. *Tumor Biol.* **1979**, *2013*, 34.
13. Wang, S.; Tabernero, L.; Zhang, M.; Harms, E.; Van Etten, R. L.; Stauffacher, C. V. *Biochemistry (Mosc.)* **1903**, *2000*, 39.
14. Manao, G.; Pazzagli, L.; Cirri, P.; Caselli, A.; Camici, G.; Cappugi, G.; Saeed, A.; Ramponi, G. *J. Protein Chem.* **1992**, *11*, 333.
15. Waheed, A.; Laidler, P. M.; Wo, Y. Y. P.; Van Etten, R. L. *Biochemistry* **1988**, *27*, 4265.
16. Wo, Y. Y. P.; Zhou, M. M.; Stevis, P.; Davis, J. P.; Zhang, Z. Y.; Van Etten, R. L. *Biochemistry (Mosc.)* **1992**, *31*, 1712.
17. Ostanin, K.; Pokalsky, C.; Wang, S.; Van Etten, R. L. *J. Biol. Chem.* **1995**, *270*, 18491.
18. Li, Y.; Strohl, W. R. *J. Bacteriol.* **1996**, *178*, 136.
19. Modesti, A.; Cirri, P.; Raugei, G.; Carraresi, L.; Magherini, F.; Manao, G.; Camici, G.; Ramponi, G. *FEBS Lett.* **1995**, *375*, 235.
20. Wo, Y. Y. P.; McCormack, A. L.; Shabanowitz, J.; Hunt, D. F.; Davis, J. P.; Mitchell, G. L.; Van Etten, R. L. *J. Biol. Chem.* **1992**, *267*, 10856.
21. Dissing, J.; Johnsen, A. H.; Sensabaugh, G. F. *J. Biol. Chem.* **1991**, *266*, 20619.
22. Bryson, G. L. M.; Massa, H.; Trask, B. J.; Van Etten, R. L. *Genomics* **1995**, *30*, 133.
23. Cirri, P.; Fiaschi, T.; Chiarugi, P.; Camici, G.; Manao, G.; Raugei, G.; Ramponi, G. *J. Biol. Chem.* **1996**, *271*, 2604.
24. He, R.-J.; Yu, Z.-H.; Zhang, R.-Y.; Zhang, Z.-Y. *Acta Pharmacol. Sin.* **2014**, *35*, 1227.
25. Jiang, Z.-X.; Zhang, Z.-Y. *Cancer Metastasis Rev.* **2008**, *27*, 263.
26. Koren, S.; Fantus, I. G. *Best Pract. Res. Clin. Endocrinol. Metab.* **2007**, *21*, 621.
27. Johnson, T. O.; Ermolieff, J.; Jirousek, M. R. *Nat. Rev. Drug Disc.* **2002**, *1*, 696.
28. Hoekstra, E.; Kodach, L. L.; Das, A. M.; Ruela-de Sousa, R. R.; Ferreira, C. V.; Hardwick, J. C.; van der Woude, C. J.; Peppelenbosch, M. P.; Ten Hagen, T. L. M.; Fuhler, G. M. *Oncotarget* **2015**, 5.
29. Wang, S.; Stauffacher, C. V.; Van Etten, R. L. *Biochemistry (Mosc.)* **2000**, *39*, 1234.
30. Zhang, M.; Zhou, M.; Van Etten, R. L.; Stauffacher, C. V. *Biochemistry (Mosc.)* **1997**, *36*, 15.
31. Zhang, M.; Van Etten, R. L.; Stauffacher, C. V. *Biochemistry (Mosc.)* **1994**, *33*, 11097.
32. Madhurantakam, C.; Rajakumara, E.; Mazumdar, P. A.; Saha, B.; Mitra, D.; Wiker, H. G.; Sankaranarayanan, R.; Das, A. K. *J. Bacteriol.* **2005**, *187*, 2175.
33. Zabell, A. P. R.; Schroff, A. D., Jr.; Bain, B. E.; Van Etten, R. L.; Wiest, O.; Stauffacher, C. V. *J. Biol. Chem.* **2006**, *281*, 6520.
34. Su, X. D.; Taddei, N.; Stefani, M.; Ramponi, G.; Nordlund, P. *Nature* **1994**, *370*, 575.
35. Homan, K. T.; Balasubramaniam, D.; Stauffacher, C. V. *PDB ID 3N8I: Structural Characterization of a secondary binding site on Low Molecular Weight Protein Tyrosine Phosphatases*.
36. Swierczek, K.; Pandey, A. S.; Peters, J. W.; Hengge, A. C. *J. Med. Chem.* **2003**, *46*, 3703.
37. Sun, J. P.; Wu, L.; Fedorov, A. A.; Almo, S. C.; Zhang, Z. Y. *J. Biol. Chem.* **2003**, *278*, 33392.
38. Khersonsky, O.; Tawfik, D. S. *Annu. Rev. Biochem.* **2010**, *79*, 471.
39. Schwender, C. F.; Beers, S. A.; Malloy, E. A.; Cinicola, J. J.; Wustrow, D. J.; Demarest, K. D.; Jordan, J. *Bioorg. Med. Chem. Lett.* **1996**, *6*, 311.
40. Dissing, J.; Dahl, O.; Svensmark, O. *Biochim. Biophys. Acta* **1979**, *569*, 159.
41. Moe, O. A., Jr.; Butler, L. G. *J. Biol. Chem.* **1983**, *258*, 6941.
42. Zhang, Z. Y.; Van Etten, R. L. *Arch. Biochem. Biophys.* **1990**, *282*, 39.
43. Moe, O., Jr.; Butler, L. G. *J. Biol. Chem.* **1983**, *258*, 6941.
44. Sun, J.-P.; Wu, L.; Fedorov, A. A.; Almo, S. C.; Zhang, Z.-Y. *J. Biol. Chem.* **2003**, *278*, 33392.
45. Hu, X.; Vujanac, M.; Southall, N.; Stebbins, C. E. *Bioorg. Med. Chem. Lett.* **2013**, *23*, 1056.
46. Mauder, D.; Akcakayiran, D.; Lesnichin, S. B.; Findenegg, G. H.; Shenderovich, I. G. *J. Phys. Chem. C* **2009**, *113*, 19185.
47. Celniker, G.; Nimrod, G.; Ashkenazy, H.; Glaser, F.; Martz, E.; Mayrose, I.; Pupko, T.; Ben-Tal, N. *Isr. J. Chem.* **2013**, *53*, 199.
48. Ashkenazy, H.; Erez, E.; Martz, E.; Pupko, T.; Ben-Tal, N. *Nucleic Acids Res.* **2010**, *38*, W529.
49. Landau, M.; Mayrose, I.; Rosenberg, Y.; Glaser, F.; Martz, E.; Pupko, T.; Ben-Tal, N. *Nucleic Acids Res.* **2005**, *33*, W299.

50. Glaser, F.; Pupko, T.; Paz, I.; Bell, R. E.; Bechor-Shental, D.; Martz, E.; Ben-Tal, N. *Bioinformatics* **2003**, *19*, 163.
51. Sohn, J.; Kristjánsdóttir, K.; Safi, A.; Parker, B.; Kiburz, B.; Rudolph, J. *Proc. Natl. Acad. Sci. U.S.A.* **2004**, *101*, 16437.
52. Lund, G.; Dudkin, S.; Borkin, D.; Ni, W.; Grembecka, J.; Cierpicki, T. *ACS Chem. Biol.* **2015**, *10*, 390.
53. Nishida, S. *J. Org. Chem.* **1967**, *32*, 2692.
54. Katritzky, A. R.; Pilarski, B.; Johnson, J. W. *Org. Prep. Proced. Int.* **1990**, *22*, 209.
55. Armarego, W. L.; Chai, C. *Purification of laboratory chemicals*, 6th ed.; Butterworth-Heinemann: Burlington, USA, 2009.
56. Still, W. C.; Kahn, M.; Mitra, A. *J. Org. Chem.* **1978**, *43*, 2923.
57. Kedrowski, S. M. A.; Dougherty, D. A. *Org. Lett.* **2010**, *12*, 3990.
58. Rajeshwaran, G. G.; Nandakumar, M.; Sureshbabu, R.; Mohanakrishnan, A. K. *Org. Lett.* **2011**, *13*, 1270.
59. Rueff, J.-M.; Caignaert, V.; Chausson, S.; Leclaire, A.; Simon, C.; Perez, O.; Le Pluart, L.; Jaffrés, P.-A. *Eur. J. Inorg. Chem.* **2008**, *2008*, 4117.
60. Kosolapoff, G. M. *J. Am. Chem. Soc.* **1945**, *67*, 2259.
61. Kosolapoff, G. M. *J. Am. Chem. Soc.* **1876**, *1949*, 71.
62. Kagan, F.; Birkenmeyer, R. D.; Strube, R. E. *J. Am. Chem. Soc.* **1959**, *81*, 3026.
63. Machida, Y.; Nomoto, S.; Saito, I. *Synth. Commun.* **1979**, *9*, 97.
64. Dixon, M.; Webb, E. C. *Enzymes*, 3rd ed.; Academic Press: New York, NY, 1979.
65. Winn, M. D.; Ballard, C. C.; Cowtan, K. D.; Dodson, E. J.; Emsley, P.; Evans, P. R.; Keegan, R. M.; Krissinel, E. B.; Leslie, A. G. W.; McCoy, A.; McNicholas, S. J.; Murshudov, G. N.; Pannu, N. S.; Potterton, E. A.; Powell, H. R.; Read, R. J.; Vagin, A.; Wilson, K. S. *Acta Crystallogr., D: Biol. Crystallogr.* **2011**, *67*, 235.
66. McCoy, A. J.; Grosse-Kunstleve, R. W.; Adams, P. D.; Winn, M. D.; Storoni, L. C.; Read, R. J. *J. Appl. Crystallogr.* **2007**, *40*, 658.
67. Murshudov, G. N.; Vagin, A. A.; Dodson, E. J. *Acta Crystallogr., D: Biol. Crystallogr.* **1997**, *53*, 240.
68. Emsley, P.; Cowtan, K. *Acta Crystallogr., D: Biol. Crystallogr.* **2004**, *60*, 2126.
69. Adams, P. D.; Afonine, P. V.; Bunkoczi, G.; Chen, V. B.; Davis, I. W.; Echols, N.; Headd, J. J.; Hung, L. W.; Kapral, G. J.; Grosse-Kunstleve, R. W.; McCoy, A. J.; Moriarty, N. W.; Oeffner, R.; Read, R. J.; Richardson, D. C.; Richardson, J. S.; Terwilliger, T. C.; Zwart, P. H. *Acta Crystallogr., D: Biol. Crystallogr.* **2010**, *66*, 213.
70. Pettersen, E. F.; Goddard, T. D.; Huang, C. C.; Couch, G. S.; Greenblatt, D. M.; Meng, E. C.; Ferrin, T. E. *J. Comput. Chem.* **2004**, *25*, 1605.
71. Humphrey, W.; Dalke, A.; Schulten, K. *J. Mol. Graphics* **1996**, *14*, 33.
72. Read, R. J.; Adams, P. D.; Arendall, W. B., 3rd; Brunger, A. T.; Emsley, P.; Joosten, R. P.; Kleywegt, G. J.; Krissinel, E. B.; Lütteke, T.; Otwinowski, Z.; Perrakis, A.; Richardson, J. S.; Sheffler, W. H.; Smith, J. L.; Tickle, I. J.; Vriend, G.; Zwart, P. H. *Structure* **2011**, *19*, 1395.
73. Wallace, A. C.; Laskowski, R. A.; Thornton, J. M. *Protein Eng.* **1995**, *8*, 127.
74. Laskowski, R. A.; Swindells, M. B. J. *J. Chem. Inf. Model.* **2011**, *51*, 2778.
75. Schrodinger, L. The PyMOL Molecular Graphics System, Version 1.3r1, 2010.
76. Shindyalov, I. N.; Bourne, P. E. *Protein Eng.* **1998**, *11*, 739.
77. McGann, M. *J. Chem. Inf. Model.* **2011**, *51*, 578.
78. Hawkins, P. C. D.; Nicholls, A. *J. Chem. Inf. Model.* **2012**, *52*, 2919.
79. Hawkins, P. C. D.; Skillman, A. G.; Warren, G. L.; Ellingson, B. A.; Stahl, M. T. *J. Chem. Inf. Model.* **2010**, *50*, 572.